Turkevich Method for Gold Nanoparticle Synthesis Revisited

J. Kimling, M. Maier, B. Okenve, V. Kotaidis, H. Ballot, and A. Plech*

Fachbereich Physik der Universität Konstanz, Universitätsstr. 10, D-78457 Konstanz, Germany

Received: March 17, 2006; In Final Form: May 24, 2006

The growth of gold nanoparticles by reduction by citrate and ascorbic acid has been examined in detail to explore the parameter space of reaction conditions. It is found that gold particles can be produced in a wide range of sizes, from 9 to 120 nm, with defined size distribution, following the earlier work of Turkevich and Frens. The reaction is initiated thermally or in comparison by UV irradiation, which results in similar final products. The kinetics of the extinction spectra show the multiple steps of primary and secondary clustering leading to polycrystallites.

I. Introduction

Noble metal nanoparticles have been intensively studied within the past 15 years. The photonic properties of gold or silver particles are appealing for materials applications,[1−3] as well as biochemical or biomedical usage.[4] Some of the interest in gold nanoparticles is a prominent optical resonance in the visible range and their sensitivity on environmental changes, size, and shape of the particles as well as the local field enhancement of light interacting with the resonant system. Therefore, applications require synthesis protocols, which deliver well-defined shapes and sizes.[5,6] Several classes of synthesis routes exist, which display different characteristics of the final products. Besides the strength of the reductant, the action of a stabilizer in the solution phase synthesis is critical. Examples of widespread usage are the organic phase synthesis after Brust,[7] involving a two phase process, or the single phase water based reduction of a gold or silver salt by citrate, introduced by Turkevich et al.[8,9] and refined by Frens,[10] which produces almost spherical particles over a tunable range of sizes. The kinetics of the Turkevich process has been addressed in a publication from Chow and Zukoski[11] focusing on the stabilization mechanism. The reduction of a golt salt in the presence of a complexing surfactant[12−14] allows us to obtain elongated, crystallographically aligned, nanorods.

Other reductants, such as amino acids, were successfully used for gold particle production without any further surfactant. The shape is delicately dependent on the reductant.[15] UV light assisted particle growth was used in the case of gold nanorods[14] or silver particles.[16] Even more direct reduction methods are provided by radiation chemistry,[17] where electrons are directly injected in the system. Even pure hydrogen has been employed to produce platinum particles[18] or silver particles,[19] which are stable without surfactant.

Ascorbic acid is frequently used for the nanorod synthesis. In this procedure, the gold ions are complexed by a surfactant molecule (such as cetyltrimethylammonium bromide, CTAB) and not directly reduced by ascorbic acid. Only the addition of gold particle seeds allows the growth of crystallographically oriented rods. This passivation can lead to a large variety of different shapes. An early study used the pure ascorbate reduction for the determination of gold salts.[20] Quite large gold particles were reported by reduction with ascorbic acid by Goia and Matijevic.[21] Jana et al.[22] have used the ascorbic acid reduction in the presence of citrate synthesized gold seeds.

Here, we focus on the citrate reduction method, which is one of the most frequently applied methods. In contrast to the original procedure, this method can also be initiated by simple UV exposure of a mixture of citrate and the gold salt at room temperature. Additionally, the usage of ascorbic acid and sodium ascorbate as a variant of the above method is similarly straightforward to produce nanoparticles already at room temperature.

The combination of optical spectroscopy, X-ray scattering, and electron microscopy, together with a kinetic study of the formation process, allows one to compare these methods quantitatively in terms of sizes and shapes of the particles.

In section IIIA we will first derive the calibration curve of sizes versus surface plasmon resonance and compare it to the Mie theory. Section IIIB will present the results of the size definition through the choice of gold and reductant concentration, and in Section IIIC, the morphologies will be discussed by means of electron microscopy and the interpretation of the extinction spectra. In Section IIID, we will present the kinetics of the particle formation, which allows us to distinguish the subsequent steps of structure formation and the influence on the particle morphology.

II. Materials and Techniques

A. Chemical Synthesis. Three approaches have been explored to produce size-defined gold nanoparticles through chemical reduction. The standard method, as described by Turkevich and Frens, is reduction by citrate at 100 °C. The reduction of a gold hydrochlorate solution (Chempur, 99%) has been initiated by sodium tris-citrate (Merck) by bringing gold solution to a boil in a double-walled reactor, which is heated by a bath thermostat. The mantle assured a very homogeneous temperature distribution within the reaction solution. The liquid is vigorously stirred by Teflon-coated magnetic bars. No refluxing was utilized in order to prevent the presence of temperature gradients in the liquid. When the solution (95 mL) started to boil, 5 mL of preheated citrate solution was added. The citrate concentration was varied to achieve different particle sizes. After a defined time (normally 15 min), the liquid was extracted and cooled to room temperature.

* To whom correspondence should be addressed. E-mail: anton.plech@uni-konstanz.de.

10.1021/jp061667w CCC: $33.50
Published on Web 07/21/2006

In addition, the reduction can be achieved at room temperature after initiation by UV irradiation. A PMMA UV cuvette (5 mm path length) was filled with 2 mL of gold hydrochlorate solution with added amounts of citrate. After stirring, the cuvette was placed in front of a UV lamp with an emission around 366 nm (15 W, Roth GmbH). The fluence of the lamp was measured to be about 1 mW/cm^2. After an exposure time from 2 to 120 min, the cuvette was placed in the spectrometer and spectra were measured repeatedly.

The third possibility is the reduction by ascorbic acid (similar results for sodium ascorbate) at room temperature. A solution of gold hydrochlorate was stirred in a reactor (49 mL), and 1 mL of ascorbic acid was added rapidly. The extinction spectra were recorded with varied delays from the mixing. For the in-situ spectroscopy, 1 mL of gold hydrochlorate solution was rapidly mixed with 1 mL of a solution of ascorbic acid directly in the cuvette, placed in the light path of the spectrometer.

A set of varying gold concentrations was tested to obtain the stability limits of the reaction.

B. Optical Spectroscopy. The optical spectra were obtained with a standard halogen lamp (Thorlabs, 150 W) and a fiber coupled spectrometer (Ocean Optics, 350−1100 nm). A 5 mm cuvette was routinely used. In the case of in-situ spectroscopy, a custom-made fiber sensor was introduced in the liquid close to the vessel wall while the vessel was illuminated from the exterior. The time resolution of the spectrometer is about 100 ms, which is faster than the speed of mixing.

The most important information in the optical extinction spectra is the intense absorption line due to the excitation of a surface plasmon resonance, which, in a dipole approximation of the oscillating conduction electrons, can be written as the following:

$$\sigma_{\text{ext}} = \frac{9V\epsilon_{\text{m}}^{3/2}\cdot\omega\epsilon_2(\omega)}{c\cdot(\epsilon_1(\omega) + 2\epsilon_{\text{m}})^2 + \epsilon_2(\omega)^2} \qquad (1)$$

with the spherical particle volume V, speed of light c, the light frequency ω, and the dielectric constant ϵ_{m} of the surrounding medium. The functions ϵ_1 and ϵ_2 describe the real and imaginary part of the dielectric function of the particle material. A resonance, the surface plasmon resonance (SPR) is expected, when the denominator of eq 1 becomes small, i.e., near $\epsilon_2(\omega) = -2\epsilon_m$.

The SPR line is homogeneously broadened due to the ultrafast dephasing of the oscillation of the conduction electrons, which has been clarified in a number of studies.[23−25] Furthermore an inhomogeneous broadening in ensembles is caused by size and shape inhomogeneities.[26] Gold particles show as well a band due to interband absorption, which is present for wavelengths shorter than 520 nm.[27] The extinction curve of a spherical particle can be quantitatively modeled by the Mie theory, which is a solution of Maxwell's equations in spherical geometry. We used the package Mieplot[28] to simulate the extinction spectra for spherical particles, which includes the full multipole expansion of the Mie formalism. One particularly useful feature of the SPR is the dependence of the position and width on the particle size. The main effect comes from retardation effects of the light−matter interaction, when the particle size approaches the wavelength of light.[1] This size effect is visible as red shift for increasing particle sizes and important for particles above 20−30 nm diameter. The extinction curve is thus an important means to determine sizes and morphology of a particle ensemble as well as for single particles. For anisotropic particles no exact solution exists; however, an extension of the Mie theory to uniaxial anisotropic particles (Gans theory[29]) is a very useful approximation for elongated particles, such as rods or ellipsoids. The general characteristics are the splitting of the SPR into two branches with polarization either parallel to the long or short axis of the rod.[30] The long axis SPR is red shifted as indicated above.

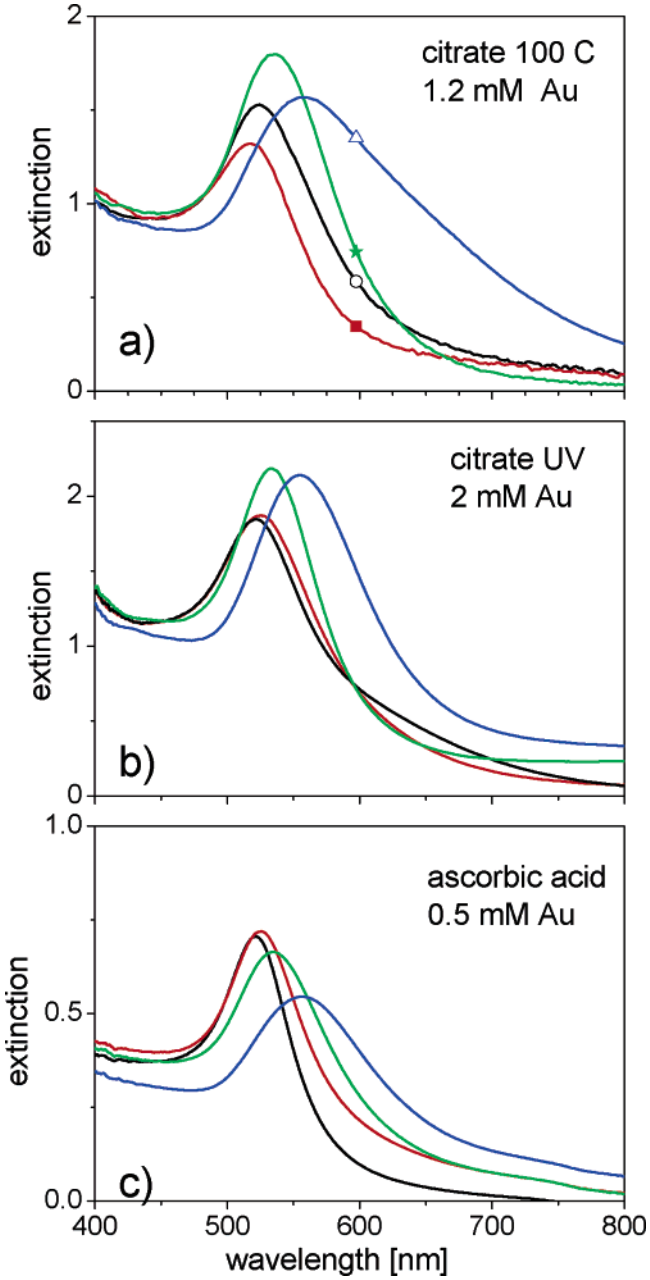

Figure 1. Extinction spectra of a set of independently prepared samples with shifted SPR due to a successive size increase. (a) Citrate prepared particles at 100 °C, (b) citrate prepared particles at 25 °C after UV illumination, and (c) ascorbate prepared particles at 25 °C.

Figure 1 shows the extinction spectra of sets of particle sizes as prepared by the three different approaches discussed in the present publication. The spectra represent the final state of the reaction at a varied reductant concentration. The SPR maximum shifts from about 518 nm up to 565 nm, while the particle sizes increase from 9 to about 100 nm (The sizes were calibrated as described in Section IIIA).

C. Scanning Electron Microscopy Analysis. The particle sizes and shapes have been derived from electron microscopy images. For the scanning electron microscopy (SEM) analysis,

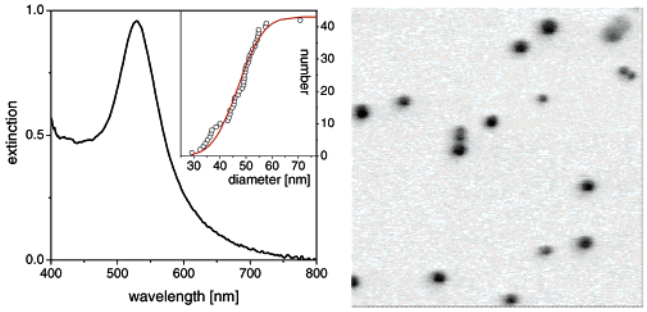

Figure 2. Extinction spectrum of gold nanoparticles prepared by UV initiation of reduction with citrate, together with a SEM micrograph of the particles supported on silicon (image size 1 × 1 μm. The inset is a plot of particle size with rank to derive the distribution function. The line is an error function fit to the data.

the particles have been adsorbed on a functionalized silicon surface. The procedure is documented in a number of studies.[31] Briefly, a silicon surface is cleaned by a mixture of concentrated H_2SO_4 and H_2O_2 in an ultrasonic bath followed by the adsorption of a monolayer of hydrocarbon molecules with silane and amino end groups (e.g., aminopropyltriethoxysilane). The amino group strongly binds the gold surface, leading to a submonolayer coverage of particles, which simplifies the inspection of particle quality and sizes. A scanning electron microscope (Hitachi) with a nominal resolution of 5 nm was used to image the surface. Gold particles show strong electron scattering compared to the substrate and are easily identified. The imaging direction is vertical to the surface. Diameters are measured for a set of particles and calibrated against gold particles with known sizes (BBI International).

Figure 2 shows a typical image of isolated particles of an average size of 47 nm. The extinction shows a well-defined SPR at 529 nm. The inset is a plot of the particle number against diameter, which, in the case of a Gaussian size distribution, can be modeled by an error function profile to determine the mean diameter and standard deviation. The standard deviation in this case was determined to be 10 nm, i.e., 21% of the mean value. Shortcomings of the microscopy technique is the limited ensemble average and the possible selectivity of the adsorption process.

D. X-ray Scattering Analysis. The small angle scattering (SAXS) has been measured at the beamline ID09B at the European Synchrotron Radiation Facility ESRF (Grenoble, France). The instrument is dedicated to ultrafast time-resolved pump probe studies and allows a flexible setup. We used the CCD detector (Mar Research, 133 mm diameter, 2048 × 2048 pixels) at a distance of 0.6 m and an X-ray energy of 10 keV. The liquid was pumped through a 0.3 mm capillary alternating with pure water.

The SAXS from the particles consisted in the difference of the two measurements. The analysis is performed by standard SAXS formulas for spherical particles[32] together with a convolution allowing for a size dispersion of the colloids. SAXS is representative for the complete ensemble of particles; however, the detailed distribution function is not generally obtainable. On the other hand, the SAXS signal is sensitive on particle−particle correlations, such as possible aggregated particles, which were not found in the present study. We could determine the sizes of particles from 9 to about 40 nm. Figure 3 shows the SAXS intensity of 35 nm particles as function of momentum transfer of the scattered X-ray $Q = 4\pi/\lambda_X \cdot \sin(2\Theta/2)$, with the X-ray wavelength λ_X and the scattering angle 2Θ. The line is a fit for spherical particles with a size dispersion

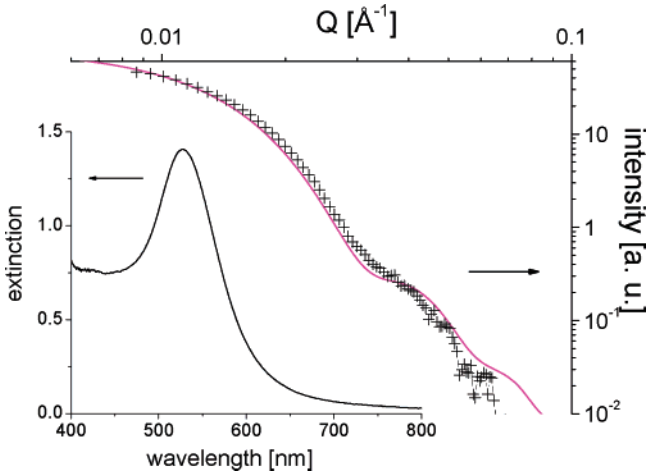

Figure 3. Small angle scattering intensity of 35 nm thermally prepared gold nanoparticles together with a simulation for spherical particles with size dispersion. The extinction shows a SPR peak at 528 nm.

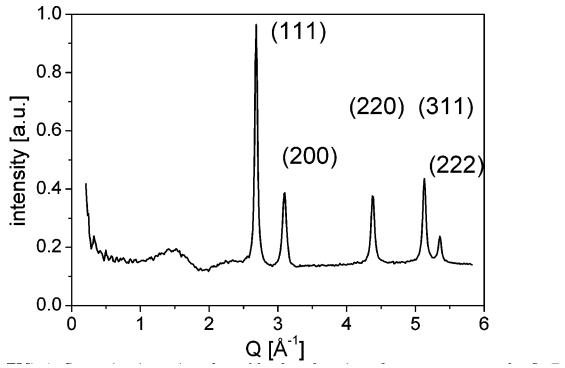

Figure 4. Scattering intensity of a gold sol as function of momentum transfer Q. The peaks corresponding to the different lattice planes in fcc gold are labeled.

of 6 nm. The inset shows the corresponding extinction curve with a SPR peaked at 528 nm. Powder scattering can be determined in a similar way, with 15 keV wavelength and a detector distance of 145 mm. The powder scattering has also partly been recorded for the particles adsorbed on a surface, as described in the previous section. Those measurements were done at HASYLAB (Hamburg, Germany, beamline D4) at 8.9 keV and with a scintillation counter.

Figure 4 shows the scattering intensity over a wide range in Q, including several reflections. The width of the (111) reflection can be used to derive the mean crystallite size through the Scherrer formula.

III. Results and Discussion

The chemical synthesis of metal particles by reduction of the corresponding metal salts is an apparently simple process, which only requires the mixing of the reagents at well defined external conditions. These conditions can affect, in subtle ways, the final morphology of the particles. We have concentrated, in the present study, on the reactant concentrations, but other parameters, such as temperature or pH value also have a strong influence on the morphology. Reducing the temperature in the thermal citrate reaction drastically affected the size and quality of the final particles toward larger diameters and irregular shapes.

A. Size Calibration of Extinction Spectra. By varying the citrate versus gold concentration for the thermal reduction

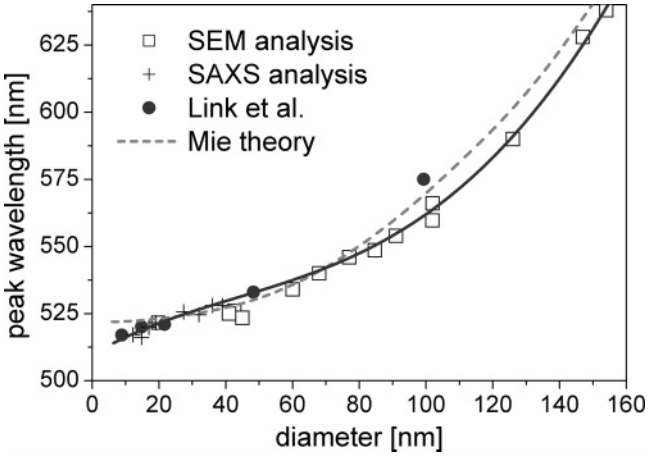

Figure 5. Diameter of citrate prepared gold nanoparticles as function of the peak wavelength of the SPR in the extinction curves. Open squares are derived from SEM, crosses from SAXS measurements, and the red dots are data taken from references. The solid line is a polynomial least-squares fit to the data points derived within the present study. The dashed line is a extraction of the peak wavelength from Mie calculations (see text).

samples with variable SPR, positions were obtained. The peak position can be correlated to the average size of the particle by a monotonic function. Figure 5 shows the relation between size and SPR position. The data for smaller particles is derived from SAXS, while the larger particles are accessible by SEM. The line is a polynomial fit to the data and can subsequently be used as calibration curve. A result from Mie calculations is compared to the data. In general the agreement between measurements and the theoretical prediction is very good. However two details are worth mentioning. First the Mie theory predicts a constant SPR for the smallest particles, which is not reproduced here. For the smallest particles, however, the assumption of the homogeneous medium may break down, as layering effects close to the surface (e.g., from the citrate shell) and probably chemical shifts could alter the index of refraction noticeably. Additionally the dielectric functions are a function of the size for very small particles, as e.g., the damping constants change with size.[1,33] This will also cause a shift of the resonance position. We are confident about the significance of our data, as the finite slope for small particles has been reported e.g., by Link et al.[34]

For larger particles a small offset between data and theory appears, which is slightly outside of the confidence interval. It is noticed, that for large particles (>120−130 nm) the theory predicts a splitting of the resonance into dipolar and quadrupolar excitation. This splitting is not visible in our samples due to the considerable size and shape dispersion for larger particles. Thus the derived SPR peak is blue shifted relative to the purely dipolar resonance, which has been used to compute the Mie curve.

B. Size Definition Through the Reductant Concentration. As Frens had already pointed out, the variation of the citrate concentration modifies the gold particle size within a large interval. In most studies, however, the gold concentration is below 0.5−1 mM. Our emphasis was to determine the upper limits for particle concentration. Figure 6 summarizes the results for the three different preparation procedures. The thermal citrate reduction indeed shifts the SPR maximum from 517 to larger wavelengths, indicative of larger particles while the citrate concentration is reduced. The explanation of this effect is the role that citrate plays in the passivation of formed gold particles. A high citrate concentration allows the stabilization of smaller

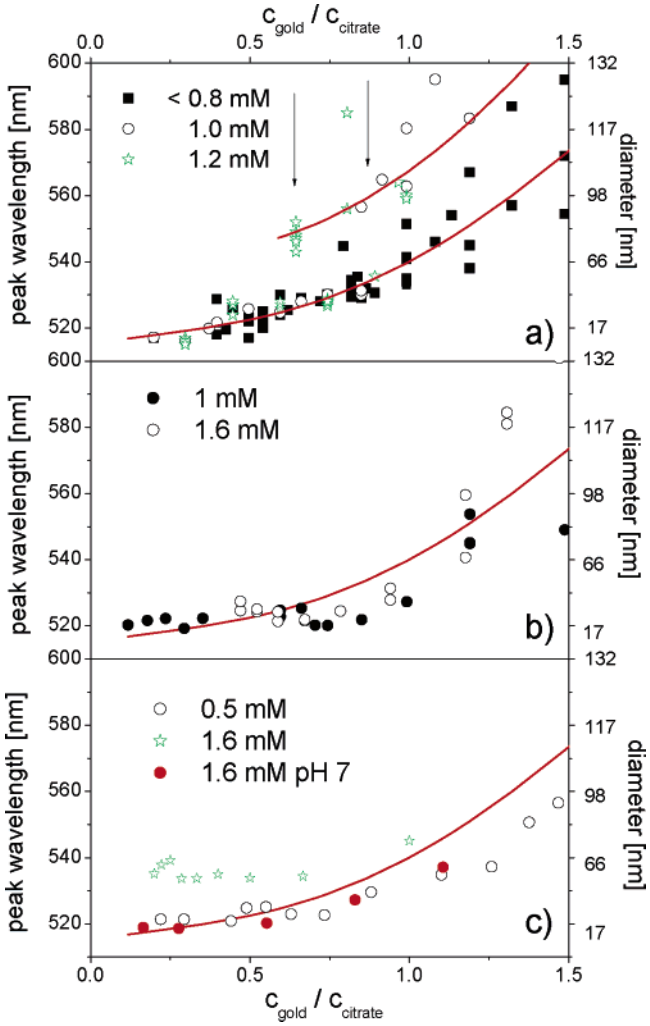

Figure 6. Peak wavelength of the SPR as function of the concentration ratios of gold ions versus reductant. (a) Citrate preparation at 100 °C. The different symbols marks the gold concentration of the liquid (■, smaller than 0.8 mM; ○, 1 mM; ★, 1.2 mM). The lines are a guide to the eye (polynomial) (b) Citrate preparation at 25° with UV illumination (5 min; ●, 1 mM; ○, 1.6 mM) with the line taken from panel a. (c) Ascorbic acid preparation at 25 °C. ○, 0.5 mM gold concentration; ★, 1.6 mM; ●, at pH 7 and 1.6 mM, with the line taken from panel a.

particles, while for smaller concentrations, the coverage is incomplete and a coarsening process leads to the aggregation of larger entities. At small gold concentrations the SPR maximum follows a general curve independent from the gold concentration, only determined by the ratio of both concentrations. In contrast increasing the gold concentration above 0.8 mM leads to a destabilization of the smaller particles and results in a size increase by almost a factor of 2. At the same time the reproducibility of the results is reduced, leading to a large variation of sizes from on preparation to the next.

This transition to larger destabilized particles shifts to a smaller gold ratio for higher gold concentration, as indicated by the arrows for 1.0 and 1.2 mM. Larger gold concentrations can in principle be used in the thermal citrate reduction, only the suspension is much less stable than for the smaller concentrations. Below 1 mM of gold ions the suspensions are stable even for months, whereas at the larger concentrations, important precipitation on the walls of the container starts within days after preparation.

In comparison, the UV initiated particle growth with citrate as reductant shows almost the same relationship between concentration ratios and SPR peak position. A larger region of

ratios exist, where the size does not vary considerably with the ratio. More importantly there is no difference for the preparation starting with 1 or 1.6 mM gold ions. Both show a similar red shift of the SPR, indicating the size increase with higher gold to citrate concentration. The increased stability during the relatively slow process (≃ hours, see section IIID) allows us to produce nanoparticles at a higher concentration than the thermal citrate reduction. The full reduction was already achieved for exposures of 3−4 min, which correspond to 1.8 (±0.6) photons per gold ion. Routinely, 5 min of exposure were used, after which the spectra were taken. Longer exposures did not change the final extinction spectrum, despite an excess signal growing with exposure time around 650−750 nm. This is an indication for a larger abundance of nonspherical particles, as will be discussed in the next section. No particle formation was observed after irradiation of the pure aurate solution without citrate.

A similar behavior to the thermal reduction is found for the ascorbate reduction at room temperature. At the 1.6 mM concentration of aurate the SPR positions are above those of the low concentration reaction (0.5 mM). Similarly the ionic strength destabilizes the small particles to form larger aggregates with shifted SPR. For the ascorbate case the destabilization is probably caused by the acidity of the solution after addition of the ascorbic acid. When repeating the same preparation with added phosphate buffer (Acros) at pH 7, the plasmon position coincides for both concentrations.

The common behavior of all three preparation routines irrespective of the differences in temperature and (with limits) from the absolute concentrations is indicative of the dominating role of the stabilizing agent compared to the general supersaturation and coarsening kinetics.[6,35] Both citrate and ascorbate are known to form a physisorbed passivation layer onto the gold particles, where the electrical double layer plays an important role in the stabilization in the suspension.

C. Structural Characteristics. Besides the average size definition in the nanoparticle synthesis the shape and size dispersion are important quantities to control. The extinction spectra of a set of small and larger particles have been correlated with the structural features in the SEM images to reveal particular imperfections and their representation in the extinction spectra. Figure 7 includes the three preparation methods.

The thermal citrate reduction results in well-defined spherical particles for the smaller particle sizes, whereas the samples with larger particles display a prominent shoulder in the extinction curve to larger wavelengths. This is indicative of a less well-defined sample quality. The electron micrographs show that indeed the particles are not round but often display elongated shapes. Inasawa et al.[36] have produced elongated gold particles with an aspect ratio about 1.3 by thermal reduction with citric acid. Also the Frens micrographs[10] show elongated particles for sizes of 97 nm and larger. It was not possible to produce samples with extinction spectra showing a symmetric SPR for the large particles as it was possible for the smaller particles. The transition from the spherical to elongated particles started at a SPR maximum around 550 nm, which corresponds to particle sizes of 85 nm. In this size region, the definition of the SPR depends very strongly on the very conditions at moment of mixing the citrate aliquot to the boiling gold hydrochlorate solution. Any temperature gradient or insufficient boiling resulted in a strong broadening of the SPR, indicative of nonuniform particle sizes and shapes.

In contrast, the UV reduction of the citrate solution and the ascorbate reduction at room temperature generally resulted in a rather symmetric SPR, as seen from Figure 7 b and c. The particles in the SEM micrograph are more spherical than the thermally prepared particles in Figure 7a. However, the UV assisted synthesis produces extinction spectra, which show a nonzero extinction baseline at a longer wavelength. The structure correlated to this feature are larger platelike particles, with an abundance of 10−15%. They often show a triangular geometry but can also be distorted hexagons. Prolonged UV exposure enhanced the signal at larger wavelengths, which points to the increased formation of platelets, similar to the formation of silver triangles by visible light irradiation, staring from spherical particles.[37]

The thermal citrate reduction would also produce a small fraction of triangles (as seen in Figure 7a, middle column), with an abundance of 5%. For the ascorbate reduction we have no indications for anisotropic particle shapes throughout the range of particle sizes prepared. However the size dispersion is of 15−18% (standard deviation), while the resonance is narrow and symmetric, close to the Mie prediction. As visible in Figure 7c, on the left, the ascorbate reduction produces, to some extent, very large particles, which do not contribute to the SPR broadening, but rather to a weak baseline. This can be seen as the liquid is rather pale, indicating enhanced light scattering. The dispersion is smallest for the smaller thermally produced particles, which can be as low as 13% in a size range from 10 to 50 nm. Larger particles in general have a larger dispersion of 15−20%. This coincides with the observation of less well reproduced particle size definition from batch to batch, as seen in Figure 6.

The crystallinity is studied for the thermally produced particles, which have been used in photoexcitation experiments with pulsed X-rays.[38−40] The size of the crystallites forming the nanoparticles is displayed in Figure 8 as function of particle size.[41] The crystal size remains smaller than the actual particle dimension in all cases, showing the polycrystalline morphology. The crystal size increases with particle size up to 40−50 nm diameter, then becomes independent of the diameter with a dimension of about 25 nm. Furthermore the distribution of the powder rings relative to a substrate surface suggests, that (111) facets are present at the particle surface, which cause a crystallographic orientation.[42]

As will be discussed in more detail in the section below on the particle formation kinetics, the crystallite size bears the history of the particle fusion through the aggregation of primary small particles.

D. Particle Formation Kinetics. The temporal evolution of the extinction has been recorded as function of time after the initiation event, which either is the addition of the reductant to the gold hydrochlorate solution or the UV irradiation. Although the different reactions proceed on distinctly different time scales (seconds for the thermal reduction, hours for the UV irradiation and sub-second burst of coloring for the ascorbate reduction), all reactions show similar kinetics. The main parameters extracted from the extinction curves are displayed in Figure 9. The figure displays the first stage of the reaction, which displays the strongest temporal changes. After the displayed time window, there is still observable narrowing and shift of the detectable SPR, which is most distinct for the ascorbate process.

Shown are the position of an, eventually appearing, SPR (through a Lorentz fit to the maximum), the extinction at 530 nm, which is a good approximation of a measure for the height of the SPR, and the extinction around 410 nm, which is unperturbed by the occurrence of the SPR. The extinction at 410 nm is sensitive to the initial absorbance of the gold

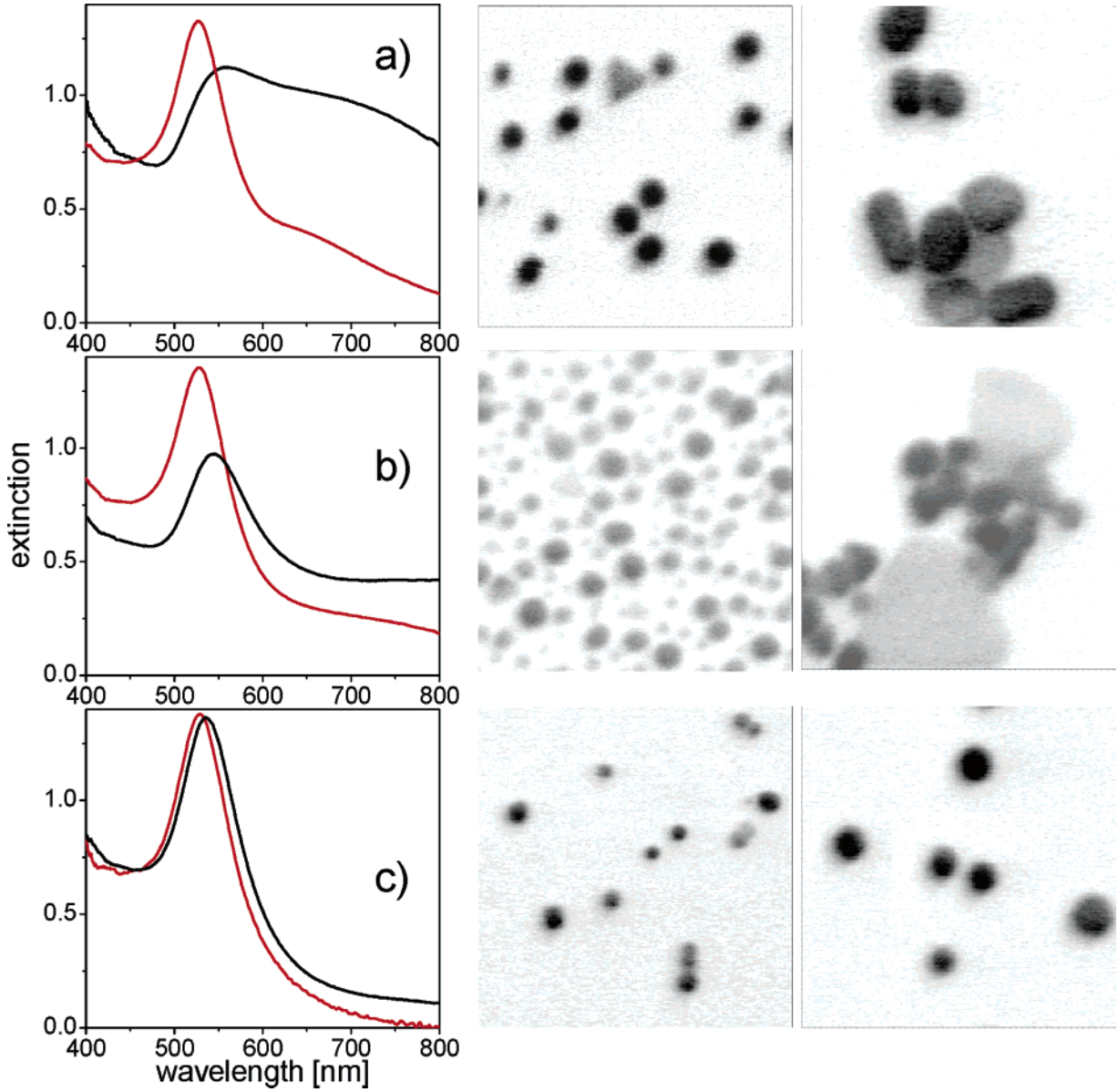

Figure 7. Optical extinction spectra and SEM images of gold nanoparticle preparations with nonideal shapes for (a) citrate at 100 °C, (b) citrate at 25 °C and UV irradiation, and (c) ascorbic acid at 25 °C. The extinction spectra each include a batch with smaller particles (black line) and one with larger particles (red line). The corresponding SEM images are the middle column (smaller particles) and right column (larger particles).

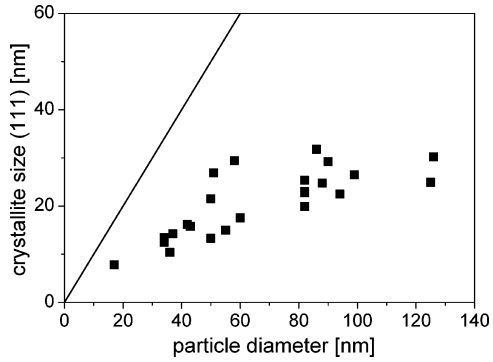

Figure 8. Crystallite size of citrate prepared gold nanoparticles as function of particle diameter as derived by the Scherrer width in powder scattering. The line indicates the ideal single crystalline relation.

hydrochlorate solution and during the appearance of nanoparticles a measure for the amount of solid-state gold material in the solution.

The kinetic traces of the thermal citrate reduction show, that immediately after the addition of the citrate aliquot to the solution, the extinction at 410 nm disappears, due the change in oxidation state of the gold ions. After an incubation period of a few seconds, the extinction slowly grows again. At this point in time, a broad, almost featureless, extinction curve is present, covering the complete visible spectrum from 400 to 700 nm. The solution shows a gray-blue tint. A maximum in the red can be quickly identified within 2−3 s shifts toward smaller wavelengths and sharpens up to the known SPR. The SPR formation is visible through the extinction at 530 nm, which is detectable after 9 s and starts to increase slowly and after 14 s more rapidly. At the same time, the position of the maximum of the SPR goes through a minimum then increases up to 550 nm before finally decreasing steadily toward the position at the completion of the reaction at 537 nm. Although the temporal evolution of the SPR position seems to be surprising at first glance, the explanation follows the known nucleation theory with a final coarsening step.[11,43]

We note that as soon as a signal at 410 nm appears, some gold atoms must have fused to form a cluster material with absorption from a delocalized band-like electron distribution.

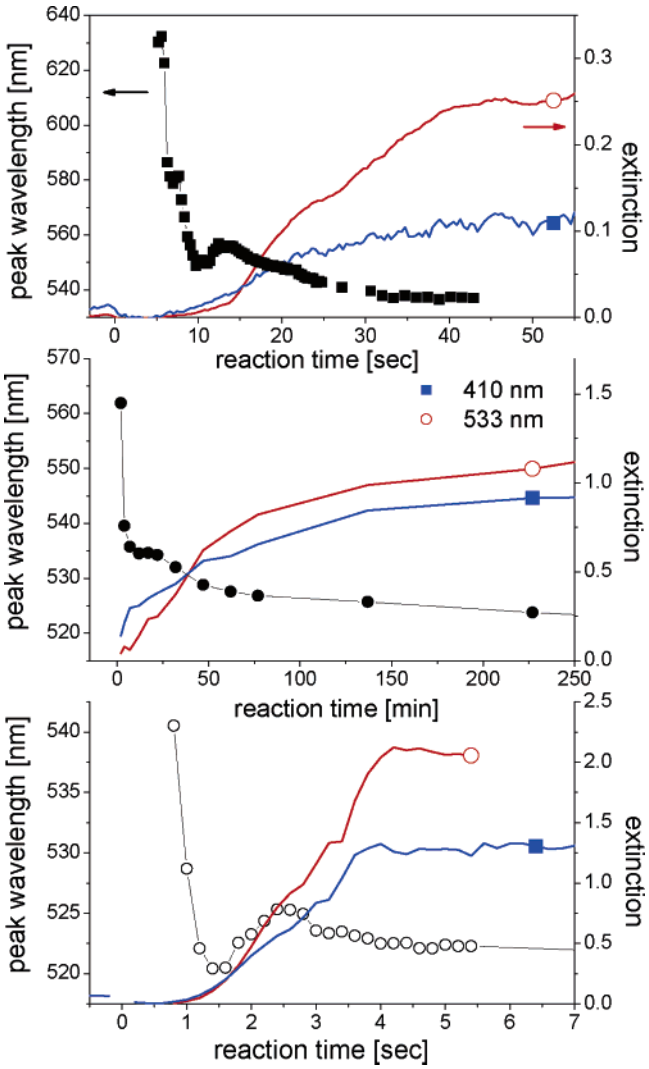

Figure 9. Time-resolved measurement of the extinction parameters of the particle synthesis from optical spectroscopy for (a) citrate at 100 °C, (b) citrate at 25 °C and UV irradiation, and (c) ascorbic acid at 25 °C. The circles mark the SPR peak wavelength, the thick line (blue) the extinction at 400 nm and the full line (red) the extinction at the peak of the SPR. Note that the time axis in panel b is minutes in contrast to panels a and c.

These clusters are presumably very small (<5 nm) and evenly distributed within the liquid. As their mutual distance is quite small, the plasmon excitation is delocalized over a large distance, which caused the broad featureless extinction over the visible range.[1] Chow and Zukoski[11] have described this first blue phase as a loose clustering of primary particles to large entities of 100 nm or more in size. They are subsequently destabilized during the growth of the contained primary particles through a change of the surface potential. In our case, the blue phase is more likely a kinetic intermediate of the reaction of undefined shape.

Based on these findings, we divide the formation process into four different regimes. The primary event of cluster formation (appearance of a broad absorption) turns into a agglomeration and compaction of the clusters into nanoparticles with a well developed SPR. It is indicated by the abrupt blue shift of the SPR position (second stage). As a third step the particles may still be unstable against fusion and form larger entities, marked by the red shift of the SPR. After this step, there are still a considerable fraction of atoms (or multiplets) present in the solution, which continue to aggregate. This is evident by the ongoing growth of the 410 nm signal. The aggregation, however, is not visible as further red-shift, but as blue-shift of the SPR. Thus the contribution of an increased size of the particles to the position of the SPR is minor in comparison to the narrowing of the SPR due to an improved symmetry and size distribution of the particles. It can be seen that the height of the SPR grows, even after completion of the gold atom aggregation. It is caused by a narrowing of the SPR, which accompanies the blue-shift. Indeed it is known, that the final particles must be compact and withstand strong elastic tension during laser excitation.[38] The homogeneous density must be formed by a continued addition of clusters and atoms to the particle surface, which fill the pores.

It is concluded that the continued reaction time after the fusion to the final particles is important for the quality of the particle shape, reflected by a narrow SPR.

The UV initiated particle growth as well as the ascorbate reduction show essentially the same features of the extinction spectra as function of time: the onset of a signal at 410 nm, accompanied by a broad feature (blue phase), which rapidly collapses to the SPR around 525−535 nm; a transient red-shift followed by a slow continuous blue shift; finally a plateau in the 410 nm signal with still increasing signal at the SPR. For the ascorbate process, which is the fastest, the steps are best separated in time. A further continuation of the SPR narrowing was observed for the ascorbate reaction in the stirred sample at high ascorbate concentration, which lasted for several hours. A similar observation has been documented during the synthesis of gold nanorods after CTAB assisted synthesis at increased pH.[44] After the growth process, the particles observed by TEM had a quite rough surface, which smoothened after several hours of reaction. At the same time the initial broad extinction curve developed two peaks as known for the nanorods.

These observations underline, that the same general growth mechanism governs the size distribution of the studied systems. The kinetics can be described in agreement with the description of Henglein and Giersig.[43] They find that silver particles are produced by pulse radiolysis with the aid of citrate as reductant, by the primary formation of small clusters, which would condense to form secondary small particles. Larger (tertiary) particles are formed by an aggregation of these secondary particles. For high citrate concentrations, the last aggregation process is less important than the Ag reduction and addition on the surface of the secondary particles, which will be enlarged, and consequently, single crystalline, while the aggregated particles at low citrate concentration are polycrystalline. Single crystalline particles were observed in the 5 nm range. Here, we find that the aggregation plays a role for all particle sizes. Consequently this discrete process will always define the size dispersion. The shape definition depends on the competing process of ion and cluster addition to the particles to form a smooth surface. For the ascorbate process this seem to be important, in view of the good sphericity of the particles.

Park et al.[35] have given a quantitative description of the kinetics of formation of monodispersed particles. The mechanism of burst nucleation involves the steps of reduction to atoms, then the formation of primary particles (<10 nm), and the final coarsening step to form micrometer sized spheres. The role of the stabilizer, however, was not taken into account, which seemed unnecessary for the chosen example of gold reduction by ascorbic acid at very high concentration (100 mM).[21] At this concentration, a similar breakdown of electrostatic stabilization, as observed here in the thermal citrate reduction, must take place. This explains the large particle sizes obtained in these

studies. The role of the continued additions of atoms to the secondary particles for the shape formation and compaction was also not discussed.

Eustis et al.[45] have observed the gold particle formation in the presence of ethylene glycol and PVP (poly-vinylpyrrolidone) after UV irradiation. They propose a chemical pathway for the reduction, where glycol acts as reductant for the excited $AuCl_4^-$ complex. There, however, the absorbance related to the Au(III) ions and the SPR peak increase both at the same pace, which is explained by a disproportionation reaction of the Au(II) ions to form neutral gold atoms. No kinetics correlated to the coarsening process was observed. The role of PVP, in contrast, as capping agent can be very different due to its polymeric character. The longer time scale for the present UV initiated growth can also point toward a slow process of formation of neutral atoms, such as the disproportionation reaction, or an autocatalytic reaction on the particle surface.

IV. Conclusion

The process of gold nanoparticle formation by the well-known citrate reduction technique has been investigated in detail and compared to its variants of UV initiated reduction and ascorbate reduction. As introduced by Frens, we have found a general relation between the gold-to-reductant ratio and the final size of the particles. This relation is, in general, independent of the absolute concentrations. The limit for the production of long-time stable particles however is below 2 mM. Even between 1 and 2 mM, gold concentration the particle sizes will be sensitive on the concentration. The size definition is best below 0.8 mM where a size dispersion of 13−16% can be achieved for particles smaller than 40 nm. Larger particles tend to develop an elongated shape, while the size definition also gets worse. The UV initiated particle growth in contrast results in more spherical like particles even at larger sizes. A small abundance of triangles and or platelets is present. The ascorbate reduction ensures the best spherical definition of the particles.

The kinetics show clear traces of a multiple step process of cluster formation, primary particle appearance, collapse to larger particles and growth of those particles by the residual amount of reduced gold in the solution. This last process is important to understand why the (polycrystalline) particles develop a spherical shape under the passivation action of the citrate (ascorbate) in the solution.

The results show that the control of the simple Turkevich process by the reduction conditions is sufficient to define particles in shape and size. Moreover this set of synthesis procedures is applicable to a much wider range of precursors, such as to form platinum, silver, or palladium particles by the choice of reductant strength and reaction conditions as temperature and UV irradiation. First positive results in the production of a manifold of particle materials by the combination of a reductant (citrate, ascorbic acid/ascorbate) and the appropriate reaction condition (temperature, UV irradiation) indicate the viability of the technique.

Acknowledgment. This project is funded by the Deutsche Forschungsgemeinschaft and the Center for Junior Research Fellows Konstanz. We acknowledge the financial support from HASYLAB.

References and Notes

(1) Kreibig, U.; Vollmer, M. *Optical Properties of Metal Clusters*; Springer: Berlin, 1995.

(2) Krenn, J. R.; Leitner, A.; Aussenegg, F. R. Metal Nano-Optics. in *Encyclopedia of Nanoscience and Nanotechnology* Nalwa, H. S., Ed.; American Scientific Publishers: Los Angeles, CA, 2003.

(3) Sönnichsen, C.; Franzl, T.; Wilk, T.; von Plessen, G.; Feldmann, J. *New J. Phys.* **2002**, *4*, 93.

(4) Hirsch, L. R. et al. *Proc. Natl. Acad. Sci. U.S.A.* **2003**, *100*, 13549.

(5) Burda, C.; Chen, X.; Narayanan, R.; El-Sayed, M. A. *Chem. Rev.* **2005**, *105*, 1025, and references therein.

(6) Cushing, B. L.; Kolesnichenko, V. L.; O'Connor, C. J. *Chem. Rev.* **2004**, *104*, 3893.

(7) Brust, M.; Walker, M.; Bethell, D.; Schiffrin, D. J.; Whyman, R. *J. Chem. Soc., Chem. Commun.* **1994**, 801.

(8) Turkevich, J.; Stevenson, P. C.; Hillier, J. *Discuss. Faraday Soc.* **1951**, *11*, 55; Enüstün, B. V.; Turkevich, J. *J. Am. Chem. Soc.* **1963**, *85*, 3317.

(9) Turkevich, J. *Gold Bull.* **1985**, *18*, 86; Turkevich, J. *Gold Bull.* **1985**, *18*, 125.

(10) Frens, G. *Nat. Phys. Sci.* **1973**, *20*, 241.

(11) Chow, M. K., Zukoski, C. F., *J. Coll. Interface Sci.* **1994**, *165*, 97.

(12) Nikoobakht, B.; El-Sayed, M. A. *Chem. Mater.* **2003**, *15*, 1957.

(13) Jana, N. R.; Gearheart, L.; Murphy, C. J. *J. Phys. Chem. B* **2001**, *105*, 4065. Jana, N. R.; Gearheart, L.; Murphy, C. J. *Adv. Mater.* **2001**, *13*, 1389. Busbee, B. D.; Obare, S. O.; Murphy, C. J. *Adv. Mater.* **2003**, *15*, 414.

(14) Niidome, Y.; Nishioka, K.; Kawasaki, H.; Yamada, S. *Chem. Commun.* **2003**, 2376.

(15) Shao, Y.; Jin, Y.; Dong, S. *Chem. Commun.* **2004**, 1104.

(16) Abid, J. P.; Wark, A. W.; Brevet, P. F.; Girault, H. H. *Chem. Commun.* **2002**, 792.

(17) Henglein, A.; Meisel, D. *Langmuir* **1998**, *14*, 7392.

(18) Narayanan, R.; El-Sayed, M. A. *J. Phys. Chem. B* **2004**, *108*, 5726.

(19) Evanoff, D. D.; Chumakov, G. *J. Phys. Chem. B* **2004**, *108*, 13948.

(20) Stathis, E. C.; Gatos, H. C. *Anal. Ed.* **1946**, 801.

(21) Goia, D. V.; Matijevic, E. *New J. Chem.* **1998**, 1203.

(22) Jana, N. R.; Gearheart, L.; Murphy, C. J. *Chem. Mater.* **2001**, *13*, 2313.

(23) Perner, M.; Bost, P.; Lemmer, U.; von Plessen, G.; Feldmann, J.; Becker, U.; Mennig, M.; Schmitt, M.; Schmidt, H. *Phys. Rev. Lett.* **1997**, *78*, 2192.

(24) Hodak, J.; Martini, I.; Hartland, G. V. *Chem. Phys. Lett.* **1998**, *284*, 135.

(25) Del Fatti, N.; Vallee, F. *Appl. Phys. B* **2001**, *73*, 383.

(26) Klar, T.; Perner, M.; Grosse, S.; von Plessen, G.; Spirkl, W.; Feldmann, J. *Phys. Rev. Lett.* **1998**, *80*, 4249.

(27) Rosei, R.; Lynch, D. W. *Phys. Rev. B* **1972**, *5*, 3883.

(28) MiePlot, http://www.philiplaven.com/mieplot.htm

(29) Gans, R. *Ann. Physik* **1915**, *47*, 270.

(30) Link, S.; Mohamed, M. B.; El-Sayed, M. A. *J. Phys. Chem. B.* **1999**, *103*, 3073.

(31) Liu, S.; Zhu, T.; Hu, R.; Liu, Z. *Phys. Chem. Chem. Phys.* **2002**, *4*, 6059.

(32) Guinier, A.; Fournet, G. *Small-angle scattering of X-rays*; John Wiley & Sons: New York, 1955.

(33) Henglein, A. *Langmuir* **1999**, *15*, 6738.

(34) Link, S.; Burda, C.; Nikoobakht, B.; El-Sayed, M. A. *Chem. Phys. Lett.* **1999**, *315*, 12.

(35) Park, J.; Privman, V.; Matijević, E. *J. Phys. Chem. B* **2001**, *105*, 11630.

(36) Inasawa, S.; Sugiyama, M.; Yamaguchi, Y. *J. Phys. Chem. B* **2005**, *109*, 9404.

(37) Callegari, A.; Tonti, D.; Chergui, M. *Nano Lett.* **2003**, *3*, 1565.

(38) Plech, A.; Kotaidis, V.; Grésillon, S.; Dahmen, C.; von Plessen, G. *Phys. Rev. B* **2004**, *70*, 195423.

(39) Kotaidis, V.; Plech, A. *Appl. Phys. Lett.* **2005**, *87*, 213102.

(40) Plech, A.; Kotaidis, V.; Lorenc, M.; Boneberg, J. *Nature Phys.* **2006**, *2*, 43.

(41) Warren, B. E. *X-ray Diffraction*; Dover Publications: New York, 1990, reprint.

(42) Plech, A.; Grésillon, S.; von Plessen, G.; Scheidt, K.; Naylor, G. *Chem. Phys.* **2004**, *298*, 55.

(43) Henglein, A.; Giersig, M. *J. Phys. Chem. B* **1999**, *103*, 9533.

(44) Wang, C.; Wang, T.; Ma, Z.; Su, Z. *Nanotechnology* **2005**, *16*, 2555.

(45) Eustis, S.; Hsu, H.-Y.; El-Sayed, M. A. *J. Phys. Chem. B* **2005**, *109*, 4811.